AIAA 98-2511

Design and Fabrication of a 9.5-inch Mach-6 Quiet-Flow Ludwieg Tube

Steven P. Schneider
School of Aeronautics and Astronautics
Purdue University
West Lafayette, IN 47907-1282

20th AIAA Advanced Measurement and Ground Testing Technology Conference
June 15-18, 1998 / Albuquerque, NM

Design and Fabrication of a 9.5-inch Mach-6 Quiet-Flow Ludwieg Tube

Steven P. Schneider*
School of Aeronautics and Astronautics
Purdue University
West Lafayette, IN 47907-1282

Abstract

A high Reynolds-number Mach-6 quiet-flow Ludwieg tube is being developed at Purdue University, based on the existing Mach-4 Ludwieg tube. The design is almost complete and fabrication is about half complete. The 9.5-inch nozzle was designed with e**N methods in order to maintain a laminar nozzle-wall boundary layer, as described earlier. The mechanical design of the nozzle is sketched. In addition, boundary-layer separation should be eliminated in the contraction and driver tube, in order to reduce residual noise that will propagate into the test section via acoustic or convective means. The contraction and bleed-lip design was carried out using the Rott-Crabtree method and an axisymmetric panel-method code. Matched cubics were used for the contraction shape, as suggested by Morel (1975). The detailed design of the driver tube, contraction, and nozzle is described.

Introduction

Brief Summary of the Need for Quiet Tunnels

Laminar-turbulent transition in high-speed boundary layers is important for prediction and control of heat transfer, skin friction, separation, and other boundary layer properties. However, the mechanisms leading to transition are still poorly understood, even in low-noise environments. Applications hindered by this lack of understanding include reusable launch vehicles such as the X-33, high-speed interceptor missiles ([18], [19]), and hypersonic cruise vehicles [1].

The noise levels present in conventional high-speed wind tunnels are 10 to 100 times higher than in flight. Because of this, conventional-tunnel measurements of both the location and the parametric trends for transition can be dramatically different from flight measurements [29, 36]. *Only the study of controlled disturbances in a controlled quiet environment can produce unambiguous data suitable for development of reliable theory.* Reliable predictive methods will have to be based on estimates of the flight disturbance environment.

The Purdue Low-Reynolds Number Mach-4 Quiet-Flow Ludwieg Tube

Quiet facilities require low levels of noise in the inviscid flow entering the nozzle through the throat, and laminar boundary layers on the nozzle walls. These features make the noise level in quiet facilities an order of magnitude lower than the 0.5 to 3 percent pressure fluctuations typical of conventional facilities. In order to reach these low noise levels, conventional blow-down facilities must be extensively modified. Requirements include a 1 micron particle filter, a highly polished nozzle with bleed slots for the contraction-wall boundary layer, and a large settling chamber with screens and sintered-mesh plates for noise-reduction [10].

To reach these low noise levels in an affordable way, the Purdue facilities are designed as Ludwieg tubes [33]. A Ludwieg tube is a long pipe with a converging-diverging nozzle on the end, from which flow exits into the nozzle, test section, and second throat (see, e.g., Figure 1 and ref. [22]).

A diaphragm is placed downstream of the test section. When the diaphragm bursts, a shock wave passes downstream, and an expansion wave travels upstream through the test section into the driver tube. The nominal end of the run occurs when the expansion wave has returned to the test section after reflecting from the upstream end of the driver tube. Since the flow remains quiet after the wave reflects, sufficient vacuum can extend the useful run-

*Associate Professor. Senior Member, AIAA.

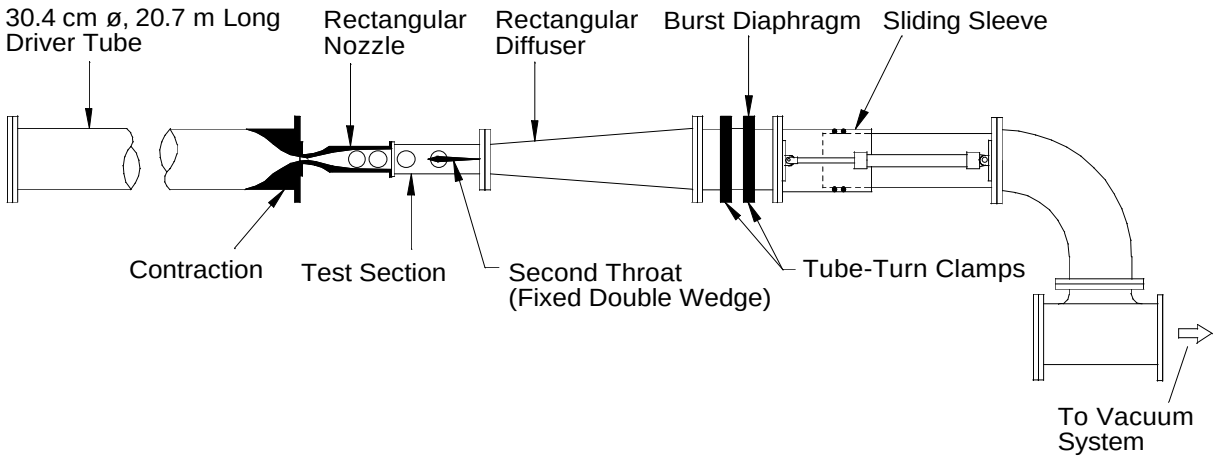

Figure 1: Schematic of Purdue Mach-4 Quiet-Flow Ludwieg Tube

time to many cycles of expansion-wave reflection, during which the pressure drops quasi-statically.

Figure 2 shows the Mach-4 nozzle of the existing low-Reynolds number facility. The region of useful quiet flow lies between the characteristics marking the onset of uniform flow, and the characteristics marking the upstream boundary of acoustic radiation from the onset of turbulence in the nozzle-wall boundary layer. The usual quiet-flow length Reynolds number is based on the unit Reynolds number in the test section, and the length on the centerline between the onset of uniform flow and the first arrival of noise radiated from the nozzle walls. For an axisymmetric nozzle with a nominally uniform transition location, this quiet uniform flow region will consist of back-to-back cones angled at the Mach angle. For most applications only the upstream cone will be useful.

Quiet-flow operation at length Reynolds numbers of about 400,000 has been demonstrated in the existing facility, making it suitable for measurements of receptivity and instability, but not complete transition to turbulence [33]. These quiet-flow results also show that the basic concept for the facility is sound. Recent work has shown that controlled perturbers and diagnostic instrumentation can be developed and operated in the facility, and that useful instability measurements can be obtained [20, 21, 31, 32].

Operation with quiet flow at higher Reynolds numbers now requires only a larger and higher quality test section. Reference [36] describes the conceptual design of the new facility, along with detailed e**N computations carried out in order to optimize the nozzle shape. The throat finish and waviness requirements are also discussed there. Here, the detailed design of the driver tube, contraction, and nozzle are discussed.

Driver-Tube Design and Fabrication

The driver tube must be large and long enough to supply a sufficiently constant pressure to the nozzle. Russell et al. review the standard theories for the drop in stagnation pressure in Ludwieg tubes, due to the growth of the boundary layer on the tube walls [30, 41]. This boundary layer is normally assumed to be turbulent. These theories have been in good agreement with high Reynolds number experiments [39]. Unfortunately, these do not give good agreement in our present Mach 4 facility, for reasons which remain to be determined. Instead, the driver tube was designed using simple isentropic relations that do give a good approximation to the driver-tube flow [37]. The driver-tube boundary layer in the Mach-4 facility may be laminar.

The driver tube must be heated to provide condensation-free Mach-6 flow, and initially there were concerns about free-convection currents that might develop in the driver tube and be swept down into the test section. Tests carried out in the Mach-4 facility showed that these were not a problem [38]. However, the paint on the carbon-steel Mach-4 driver tube flaked off during the thermal cycling, so the new driver tube had to be made from stainless steel. Rigorous cleanliness is absolutely critical, since small amounts of oil or grease condense in the throat of the nozzle as the air cools, and small amounts of particles also deposit there. Sufficient dirt buildup eliminates quiet flow.

The driver tube that was fabricated consists of 122.5 ft. of 18-inch schedule 10 stainless-steel pipe, type 304L. The internal diameter is 17.5 inches, with a 1/4-inch wall, and the tube is ASME U-stamped

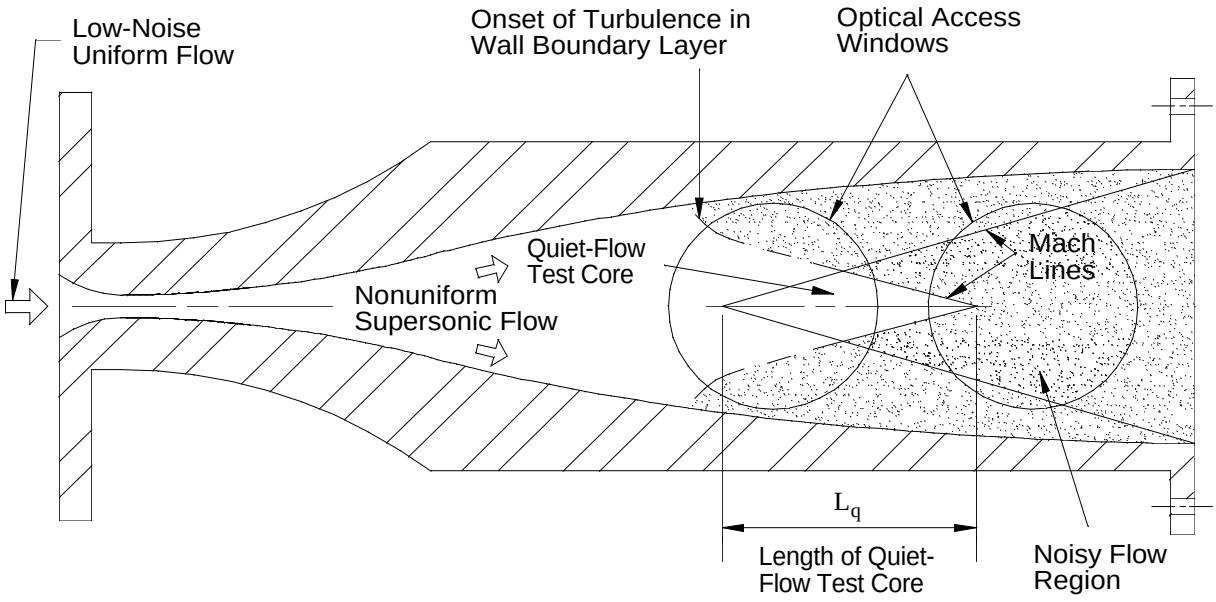

Figure 2: Schematic of Existing Mach-4 Quiet-Flow Nozzle

for 300 psig at 392F. The diameter is large enough to allow a person to crawl through and clean the inside, a critical requirement. A 140-ft driver tube was initially planned, but the 24% pressure drop computed for a 7 sec. runtime was only slightly better than the 27% computed for a 120-ft. driver tube.

Transition of the Driver-Tube Boundary Layer

Transition in the boundary layer on the driver-tube wall is a major uncertainty in the design of the present facility, and may be one of the causes for the discrepancy in the pressure-drop computations. Transition is also a concern for nozzle quietness, since fluctuations generated in the driver tube can enter the throat of the nozzle through acoustic or convective means. A blip of noise has been observed in the present Mach-4 facility at about 0.8 s into the run, and never explained. Although the usual methods for computing the pressure drop in Ludwieg tubes assume a turbulent boundary layer, theories based on a laminar boundary layer also exist [7, 8, 14].

Amr et al. made measurements of transition on the walls of a rectangular tube into which an expansion wave propagated [3]. The tube was 1.5 by 5 inches, and had a 3.5-ft. polished section. Transition was detected on the polished surface using hot wires and surface hot films. Transition occurred at displacement-thickness Reynolds numbers ($Re_{\delta^\star}$) that scattered between 4000 and 8000. Barrand et al. made measurements in a glass tube with a 5 cm i.d. [6], using dynamic pressure transducers mounted flush with the wall. The pressure is plotted versus time, and transition is inferred at a sudden change in slope; this inference was confirmed using hot-wire fluctuation measurements. Transition occurred at $Re_{\delta^\star} = 7200$.

Piltz made measurements in a Ludwieg tube which had no contraction [26]. He shows a rise in test-section pressure fluctuations when the driver-tube turbulent boundary layer is swept past the sensor. Page 4 in Ref. [27] shows data for boundary-layer transition on a driver-tube wall at an arc-length Reynolds number of about 3.5 million. The pressure drop was smaller when the boundary layer was laminar. Since the driver-tube was constructed of seamless brass pipe with special interconnecting tapered sleeves, this Reynolds number is probably toward the high end of what might be observed [25].

In the Purdue Mach-4 tunnel, a blip of noise is often seen, about 0.8 s into the run. At this point, at the usual stagnation pressure of 1 atm and driver-tube Mach number of 0.0069, the arclength Reynolds number, Re_s, for the driver-tube boundary layer is only about 90,000. In view of Piltz's results, it seems unlikely that the driver-tube boundary layer has transitioned. For a zero-pressure gradient laminar boundary layer at $Re_s = 100,000, Re_{\delta^\star} = 544$, and we are far below the smooth-wall transition data from any of the experiments. Although the Mach-4 facility has a joint at the upstream end of the contraction, and another joint between pipes 8 ft. up-

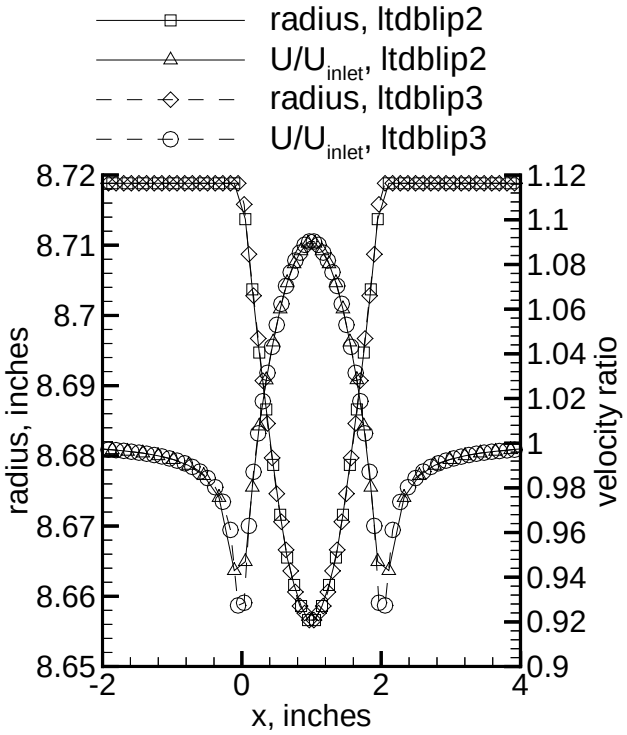

Figure 3: Potential Flow Past a Wave in the Driver Wall, Two Resolutions

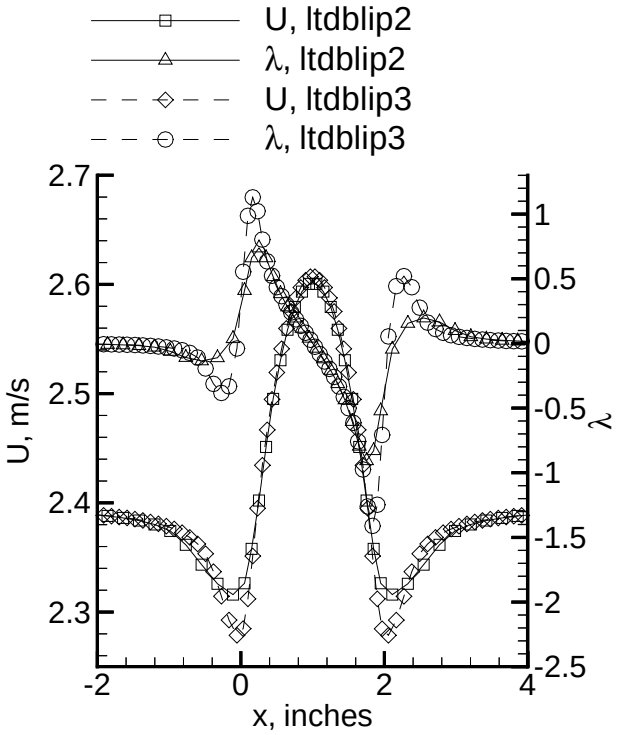

Figure 4: Boundary-Layer Separation on a Wave in the Driver Wall, Two Resolutions

stream of the contraction entrance, the contraction joint provides a step that is about 0.005 inches or less, and the boundary layer is probably laminar entering the contraction.

The new Mach-6 facility has a design pressure of 10 atm. and a design stagnation temperature of 440K. The tube Mach number is still very low, about 0.003. At the end of a nominal 7 sec. run, $Re_{\delta^\star} \simeq 3200$ using Blasius, which suggests that the driver-tube boundary layer may remain laminar, if the roughness is sufficiently small.

Control of Boundary-Layer Separation in the Driver Tube

To help keep this boundary layer laminar, and to reduce the chance of boundary-layer separations that could also lead to test-section noise, the steps and gaps at the joints in the driver tube were made as small as possible. The schedule 10 stainless pipe comes in 20 foot random lengths.

The risk of separation caused by flaws in the tunnel wall is explored in Figures 3 and 4 Figure 3 shows a wave in the wall of a tube with a 17.5-in. inside diameter. The wave has an amplitude of 1/16 in. and a length of 2 in., and consists of half of a sine wave cycle. The potential flow is computed with the PMARC code, as in [34]. The small wave generates a fluctuation in the surface velocity of about $\pm 10\%$. Both cases use 19 panels around the half-circumference of the axisymmetric pipe, and assume symmetry. In both cases, the upstream boundary is 1 radius upstream of the beginning of the wave, and the downstream boundary is 1 radius downstream of the end of the wave. Case `ltdblip2` has a total of 2565 panels, and case `ltdblip3` is higher resolution, with 4275 panels. The two grids agree well.

Figure 4 shows the same surface velocity data along with a Rott-Crabtree computation of the pressure gradient parameter λ, which equals -0.09 at laminar separation. Both grids show $\lambda < -0.8$, a strong indication of separation. The differences between the grids show up more in the derivative λ, but the agreement is still good. Fairly small waves in the driver-tube wall can clearly lead to local boundary-layer separations, which from the λ curve may only be a fraction of an inch long.

The initial concept called for joints using a full-circumferential butt weld, which would then be ground on the inside to create a smooth surface. However, when this was tested with a short piece

of pipe it worked poorly. The pipe is out of round as it arrives from the mill, by varying amounts up to perhaps 1/8 inch. When the test pipe was cut to make the joint, it springs to a different shape. Although a jig was machined to squeeze the pipe as round as possible before welding, the weld joint still has smoothed-out steps, and a 12-inch straightedge rocks as much as about 1/8 inch when placed over the joint. In view of the above computations, this wave was a concern.

Custom flanges were therefore machined for all the joints. The flanges seal with o-rings and mate using 2 dowels. The inside diameters were matched to within a few thousandths after machining. The flanges were bored out so that the pipes could be inserted before welding. Unfortunately, the minimum bore size into which the pipes could successfully be inserted was still about 1/16-inch larger than the pipe outside diameter. Fortunately, the welding process pulled the pipes so they were more round. The same process reduced the accuracy of the flanges, however. The flanges were hand-finished after welding to smooth out the inside weld, and although this finishing was to be kept away from the matching surfaces the accuracy was further reduced.

The end result has a small streamwise wave near the inside weld, with a radius increase of about 0.050 inches over a length of about 1 inch, the larger radius being in the middle of the flange. The inside diameter at the downstream end of the overall assembly varies from a maximum of about 17.511 to a minimum of 17.467, in a slightly elliptic pattern. The joint between this last pipe and the next one upstream was measured after assembly to have a step that varies from 0 to about 1/32-inch. There is a corresponding gap at the joint, where the edge had become somewhat beveled. Boundary-layer separation may occur at these joints, but they had to be accepted. Improvements will require hand work from the inside.

Contraction Design

The design of the nozzle and contraction incorporates the use of a boundary-layer bleed slot just upstream of the nozzle throat, as in Langley designs [43]. Although the large accelerations present in the contraction would probably laminarize any turbulence present in the boundary layer entering the contraction, it still seems possible that without the suction-slot, some residual disturbances might convect into the nozzle and cause earlier transition. The suction slot starts the nozzle-wall boundary layer at a fresh and known location. If the upstream flow is attached and steady, then the flow in the contraction should be smooth and steady, and the disturbance level entering the nozzle-wall boundary layer at the bleed lip should be small.

Disturbances generated in the contraction-wall boundary layer by the steps and gaps at the joints are sucked away, assuming that the slot is sufficiently wide. The noise radiated onto the bleed lip by the fluctuations in the contraction-wall boundary layer should be small, since the flow there is subsonic. However, substantial contraction-wall separations must be avoided, even in subsonic low-noise tunnels, since they can be a substantial source of noise. Computations similar to the ones shown below were performed for the Langley Mach-6 quiet tunnel, and they suggest that separation probably occurred in the short contraction used. Thus, separation in the contraction may be partially responsible for the residual low-frequency noise measured there [45].

The bleed slot must be designed to have sonic flow on the suction side, to avoid the transmission of fluctuations from the suction piping through the slot [4, Figure 21]. These would then cause fluctuations in the bleed-lip stagnation point, and thus disturbances in the nozzle-wall boundary layer. Separations from the bleed lip itself must also be controlled, for similar reasons. Although the bleed slot adds complexity, cost, and risk, on balance it seems preferable to problems that may occur when it is omitted.

Selection of Analysis Method

The original plan was to compute the flow in the contraction and bleed slot using the Strikwerda Navier-Stokes code [40, 5]. This code was specially written to compute the flow in slotted axisymmetric nozzles, and reference [5] contains results for the Langley Mach-8 quiet nozzle. One of the latter figures in reference [5] does show a detail of the flow around the bleed lip, but the resolution is very limited (for example, the tip is represented as a triangle, not a hemisphere). Although the code was successfully ported to a PC, it is poorly documented, and grid-independent results were never successfully obtained. Since, in addition, it appeared impossible to use this code to compute separations in the nearly-incompressible contraction inlet, a different code was sought.

The flow near the bleed slots of the Langley Mach-8 quiet nozzle was also computed using CFL3D [9, Figure 12b]. However, the paper shows only some low-resolution contours in the main flow, with no detail near the lip or in the boundary layers.

The lip is located at a Mach number of about 0.14; further details from this computation are apparently not available. The use of this code was not pursued since: (1) the code is complex and requires use of expensive hardware, (2) the bleed lip is at a Mach number of 0.5 or less, and so can be analyzed with incompressible methods, (3) the transonic throat flow is already analyzed as part of the nozzle design, and (4) a code that can compute the incompressible flow in the inlet entry is needed, to determine if inlet separation exists.

In 1992 the Ames 3D panel-method code PMARC was used to analyze the contraction of the Mach-4 nozzle [34]. However, it was very difficult to grid the (primarily) axisymmetric contraction with a 3D code, and still achieve accurate and smooth solutions. The Rott-Crabtree method was used to analyze the laminar boundary layer; this method is the axisymmetric analog to the better-known Thwaites method [42, p. 297]. It requires differentiating the inviscid surface velocity in order to determine the pressure gradient. When this differentiation is carried out, even after smoothing, the results for the pressure-gradient parameter λ were very irregular [34].

To obtain smoother solutions with less computational effort, an axisymmetric panel-method code was obtained from Danny Hwang at NASA Lewis. This code, EOD2, was written by Hess, Martin, and Friedman at Douglas Aircraft [16, 13]. Reference [17] discusses the method in detail. Since the code is written for axisymmetric flow, the axisymmetric effects are already resolved (through elliptic integrals), and it is only necessary to supply the streamwise and radial coordinates. The code uses a 2nd-order panel method, and generally computes the required panel curvatures internally. The code was converted from FORTRAN-66 to FORTRAN-77 using a commercial automatic-converter program, `FOR_STRUCT`, after which the format of the input and output were modernized, and the array sizes were increased.

The Rott-Crabtree method was again used to analyze the boundary layer on the contraction walls. This assumes a laminar boundary layer, which for separation purposes should be the worst case. Boundary-layer computations shown below indicate that for many conditions the boundary layer is likely to be laminar in the contraction.

Validation of the Hess Axisymmetric Panel-Method Code

The sphere test-case supplied in the manual was first exercised; the results agreed with those given in the manual, to 3-5 significant figures. A series of sine-shaped contractions were then tried, with results similar to those shown in Figure 8 of reference [16]. The code allows computation of the velocity field for a simulated rake of measurement points. By placing such a rake across the entire contraction, the integrated massflow can be readily computed, and the massflow at different streamwise positions checked. When 726 points were used to simulate a 12:1 sine-shaped contraction, the massflow was consistent to within about 0.6%, except near the ends of the inlet and exit. Since the velocity ratio is 144, this suggests there is good accuracy even in the computation of the low-speed velocities. The runtime was about 4 minutes on a 180 MHz Pentium.

With an inlet length of about 4 inlet radii (726 panels), the massflow agreed to about 0.7%; when this length was increased to 6 radii (968 panels), the agreement improved to about 0.6%. There was a shift in the (arbitrary) absolute velocity of as much as 10% between these two runs, but the shape and derivatives were very similar. It is important to have sufficient panels, and limited variations in panel size; when the number of panels in the 12:1 contraction were reduced in half, keeping the inlet length at about 5 radii, the massflow consistency was reduced to 3%.

When run in double precision, the code actually runs quicker than in single precision, presumably because the floating point operations on a Pentium chip are normally carried out on an 80-bit floating point processor anyway. Double precision was therefore used for most runs, although it required the use of more disk space. When single precision was used with contraction ratios of more than 100, waviness problems were noted in the low-speed velocity distributions. The code uses disk space for interim storage; a run with 1500-2500 panels requires the use of roughly 200-400 Mbytes of disk space, and executes in roughly 20-40 minutes on a 180 MHz Pentium.

The massflow conservation and the derivatives of the surface velocity are sensitive to accurate positioning of the panels. When externally-generated panel curvatures were supplied for the same 12:1 sine-shaped contraction described above, using analytical methods, the massflow consistency improved from 0.6% to 0.03%. When the sine-shaped contraction flattens out into the straight inlet or exit, the internally-computed curvatures gave rise to a 10% velocity fluctuation at the 2 panels nearest the joint; this fluctuation disappeared when externally-generated curvatures were supplied. Since the curvatures were usually computed internally, the massflux agreement in most of the cases shown below remains at about 0.6%. More panels are required

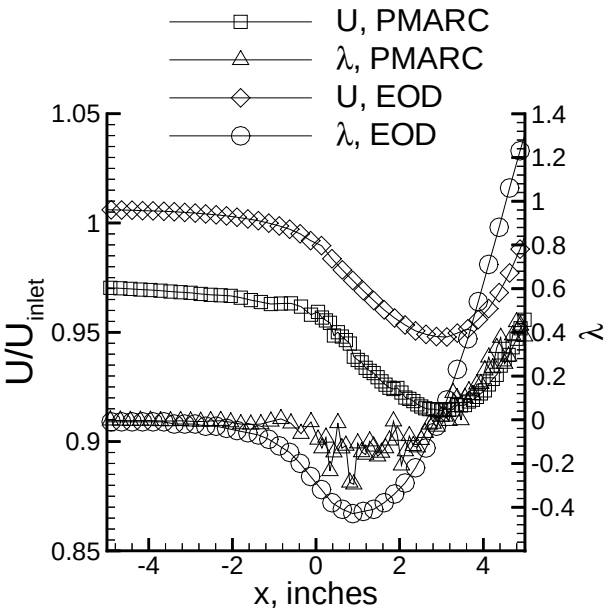

Figure 5: Contraction of Mach-4 Nozzle Computed Two Ways

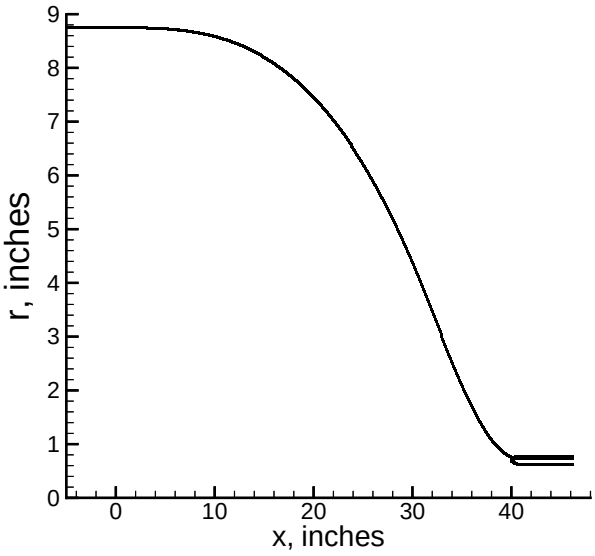

Figure 6: Overall Shape of Contraction, Final Design (m6m1y2)

for larger contraction ratios in order to achieve the same consistency of massflow; this is not surprising since the velocity ratios become very large.

Control of Separation in the Contraction Inlet

In the inlets of contractions, a local adverse pressure gradient occurs, since the pressure must be higher at the outside of the turning fluid. To keep this gradient small enough to ensure an attached boundary layer, the contraction must be lengthened [23, 11]. Morel [23] proposed the systematic use of a pair of matched cubics, to describe the contraction. His page 6 states that the required contraction length, in terms of inlet diameters, *decreased* with contraction ratio. However, Morel only studied contraction ratios from 2 to 25.

As a test of the performance of the EOD code, the flow in the contraction of the existing Mach-4 quiet nozzle was first computed. This contraction has an inlet diameter of 12 inches, and an area ratio of 83 [34]. Figure 5 compares the velocity and the Rott-Crabtree pressure gradient parameter λ. The contraction begins at $x = 0$. The axisymmetric EOD computations are clearly far smoother than the 3D PMARC computations. The minimum value of λ is about -0.5, far more adverse than the marginal separation value of -0.09. For both analyses, 7-point center-weighted smoothing is applied to the inviscid velocities before the derivative is taken. As suspected and discussed in reference [34], this existing contraction is probably too short to avoid separation. It was not possible to lengthen it, due to lack of funds. This inlet separation may contribute to the residual noise observed in the tunnel when the nozzle-wall boundary layers are laminar [20].

Contraction Geometry

Figure 6 shows the shape of the contraction, in this case with the final length of 40 inches. The inlet radius is 8.75 inches (to match the 18-inch schedule 10 driver tube), and the exit radius is selected to fit the bleed lip of the 9-inch Mach-6 nozzle described in reference [36]. Note the expanded scale on the vertical axis. The matched cubics suggested by Morel are used, between the inlet and the match to the bleed lip. The figure shows the full geometry with bleed lip and bleed slot. It is possible to analyze this with the EOD code since it is capable of analyzing multiple 'bodies'. The slope and curvature at the beginning of the inlet are taken to be 0.0. The cubics are matched through 2nd derivatives at the match point.

Figure 7 shows a detail of the geometry near the bleed lip. The upper surface of the bleed lip is parallel to the tunnel centerline, in order to ease fabrication. Simple assembly and disassembly also eases the periodic cleaning which is necessary to maintain quiet flow. A relatively short bleed lip is used [36], with a small entry angle of about 7.1 degrees. The massflux is computed for the nozzle throat assuming

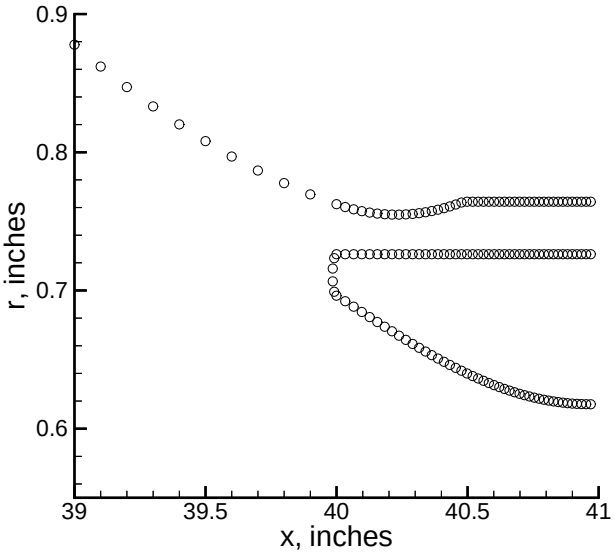

Figure 7: Detail of Bleed-Slot Lip, Final Design (m6m1y2)

uniform Mach-1 flow, and the amount of massflow to be sucked through the slot is then specified. Figure 7 shows the final design, in which 10% of the incoming massflow is to be sucked through the slot. The design is based on a 1-D inviscid streamtube analysis, as used by Beckwith [2]. Because the bleed-slot tip has finite thickness, and because the upper surface of the contraction should be smooth going past the bleed lip, there is a discontinuity in the 1-D Mach-number at the bleed lip. The contraction radius upstream of the lip is sized to accomodate the massflow through the main nozzle and the slot, plus an increase in radius to adjust for the area blocked by the tip.

With 10% suction, the slot inlet is 0.036 inches wide, comparable in size to the 0.030-inch diam. bleed lip. If the bleed lip stagnation point is at the geometric tip, the slot will intercept the first 0.051 inches of the flow near the wall. The tip diameter is nearly as small as can be fabricated accurately, and is the same as that used in the Langley Mach-8 quiet nozzle (Steve Wilkinson, private communication). It also provides sufficient wall thickness to resist hoop stresses and buckling, with a safety factor of more than 4. The slot minimum is 0.029 inches. The angle of the centerline of the lip is matched to that of the incoming streamline that stagnates on the lip, to keep the streamlines as smooth as possible. This angle is determined using the angle of the contraction at the lip, by assuming a linear distribution of streamline angles between the contraction and the centerline. The panel edges are shown as individual points - the panel spacing must be kept fairly uniform to obtain reasonable accuracy.

The 2nd derivative of the contraction at the bleed lip is not specified but results from the matched cubics. A circular arc continues the upper surface of the bleed slot, from the base of the hemispherical tip at $x = 40.0$ inches, where $x = 0$ at the contraction inlet. The arc is matched in slope to the contraction slope at that point. The slot height at the slot minimum is the third parameter needed to fix the arc location and radius. The arc continues past the minimum to the height needed to result in the correct EOD massflow, as discussed in the following. The details of the mechanical design in the region past the slot minimum are shown in Figure 25.

Bleed Slot Height Specification

The bleed slot height must be sufficient to remove the entire boundary layer, including any residual fluctuations near the boundary layer edge. Excessive slot height increases the amount of massflow that bypasses the test section, and reduces runtime.

Boundary-layer computations were carried out for the design contraction, using the Harris finite-difference code [15]. The boundary-layer was assumed to begin zero or 87.5 inches upstream of the contraction inlet. The actual start depends on the time during the run, with the latter corresponding to a time approx. 2 sec. into the run, using the contraction flow velocity of 1.3 m/s. The wall was assumed isothermal at 815R, very near the design stagnation temperature of 820 R.

Frank Chen used a similar procedure for the NASA Langley quiet nozzles. The bleed-slot entrance height was taken to be the distance from the wall to the stagnation point on the bleed lip. It was sized using a calculation of the 99.5% boundary-layer thickness (private communication, 6-5-98), and a safety factor of 1.5 to 2 [44].

Figure 8 shows the results for the 99.5% edge thickness, for a variety of driver-tube pressures and fetches. Some cases are fully laminar, while others assume the flow is always turbulent. Figure 9 shows similar results for the displacement thickness.

The worst case boundary-layer thickness results from a turbulent boundary layer at the lowest operating pressure. For an assumed 15 psia stagnation pressure, the 99.5% boundary layer thickness at the contraction exit is 0.041 inches, independent of the upstream origin of the boundary layer, with a displacement thickness of 0.005 inches. The slot height is 1.24 times the edge thickness, and the displace-

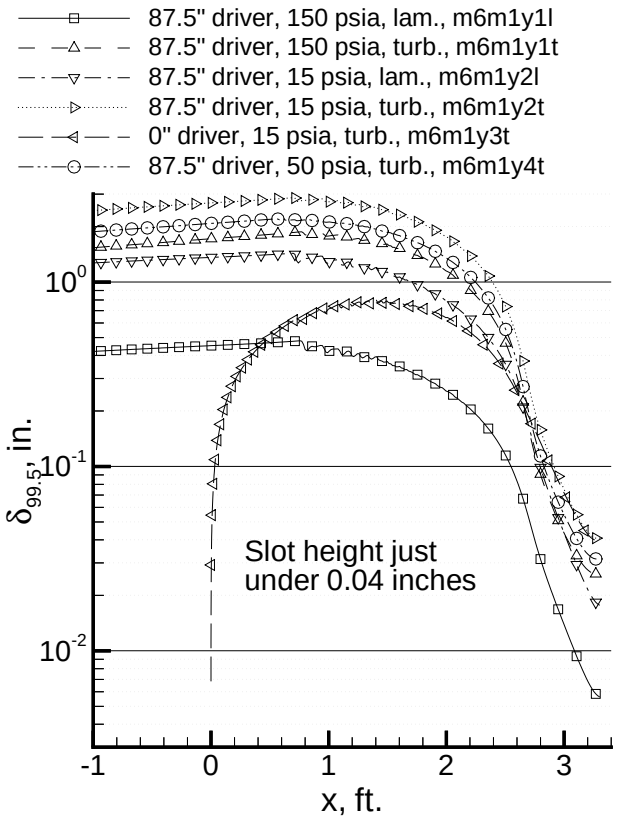

Figure 8: Contraction Boundary-Layer Edge Thickness, Final Design

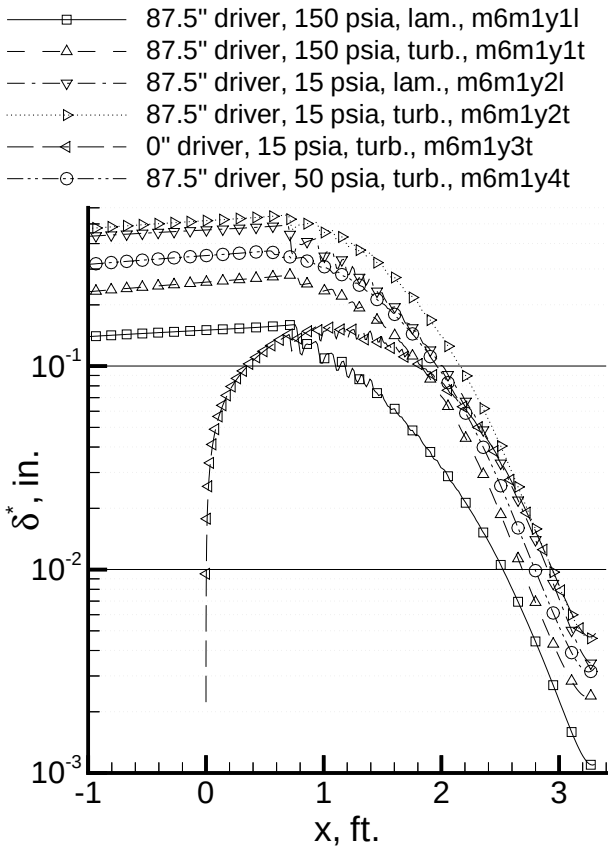

Figure 9: Contraction Boundary-Layer Displacement Thickness, Final Design

ment thickness causes a 10% error in the inviscid design (which was not corrected for). However, the laminar layer is significantly thinner at this pressure. For the laminar layer at 15 psia, the displacement-thickness Reynolds number, $Re_{\delta^\star}$, is 480 at the contraction exit, and 520 at the contraction inlet, so the boundary layer is likely to remain laminar at this pressure. The contraction thins the boundary layer dramatically (see also Ref. [34]). This thinning is essential to reasonable operation of the suction slot.

At the design stagnation pressure of 150 psia, a laminar boundary-layer assumption results in a 99.5% thickness of 0.006 inches at the slot inlet, and a 0.001 inch displacement thickness there. This would provide a large factor of safety. The boundary layer will tend to laminarize in the contraction, since although $Re_{\delta^\star}$ is 1680 at the contraction inlet, and 1520 at the contraction exit, there is a strong favorable pressure gradient. The peak value of the relaminarization parameter $K = \nu(dU/dx)/U^2$ is roughly 4×10^{-6}, suggesting that relaminarization in the contraction is likely but not assured [24].

To be conservative, turbulent flow was then assumed at the boundary-layer origin, still at 150 psi. At the contraction inlet, $Re_{\delta^\star}$ is then 2900, and $Re_x \simeq 1 \times 10^6$, so the flow may or may not be turbulent there. At the end of the contraction, $Re_{\delta^\star} = 3500$, so the flow may still be turbulent, with $\delta^\star = 0.0025$ inches and a 99.5% thickness of 0.027 inches. This allows a safety factor of nearly 1.9, within the 1.5 to 2 range used by Langley [44]. The 99.5% thickness at the contraction inlet is 1.7 inches, so again the effect of the contraction is essential in thinning the boundary layer and possibly laminarizing it.

The '0" driver' plot in the figures shows the effect of starting the boundary layer at the contraction inlet, simulating a time early in the run. The boundary layer thicknesses at the contraction exit differ by only a few percent, showing the dominant effect of the accelerations.

However, the fetch of the boundary layer may still have a significant effect, since a high Reynolds-number thick turbulent boundary layer at the contraction entrance would seem more likely to leave

fossil turbulent fluctuations in the outer regions of the contraction boundary layer, which might conceivably convect past the bleed lip into the main part of the flow. Since the radius has contracted from 8.75 inches to 0.76 inches at the bleed lip, the area has contracted by a factor of 133 here. A one-dimensional analysis suggests that the area of this 'fossil' boundary-layer should also contract by a factor of 133, or that the height contracts by a factor of 11.5. Since the 99.5% thickness at the contraction inlet for the base 150 psia turbulent case is 1.7 in., this suggests a fossil-boundary-layer thickness of 0.15 inches at the bleed lip, a value too high to capture with the kind of bleed-slot design used here. If this effect is real, quiet flow will terminate early in the supersonic run, at high pressures, due to fluctuations passing the bleed lip in this manner. No effect of this type has been seen in the present Mach-4 facility, but it is possible that the driver-tube boundary layer is always laminar at the lower Reynolds numbers present there.

If the stagnation pressure is reduced to 50 psig, a low operating value, and the boundary layer is again assumed turbulent, the 99.5% thickness at the slot inlet is 0.032 inches, which still provides a safety factor of 1.6. At the contraction inlet, $Re_{\delta^\star} = 1280$, and $Re_s = 320,000$, so the boundary layer is likely to be laminar, and the turbulent assumption is conservative, at least early in the run.

The 10% bleed-slot suction selected thus seems a reasonable compromise. Late in the run, when the tube-wall boundary layer has built up, it is possible that difficulties may occur, although this boundary layer is dramatically thinned in the contraction. At lower pressures, it is possible that conditions may arise when the contraction-wall boundary layer is thick and turbulent and not all of it is sucked off. However, the risk of this appears small. A replaceable slot-throat ring is incorporated in the mechanical design to ease adjustments of the slot minimum, but it is not large enough to allow adjustment of the slot entry height. However, a minimal recut of the last section of the contraction could allow an increase in the slot entry height. The suction air passes through a plenum and eight 1-inch hoses to two 2-inch vacuum lines, which are sized to produce a pressure drop that is less than 10% of the pressure drop across the sonic jet.

Length of Contraction

A longer contraction reduces the chance of boundary-layer separation in the entry, and results in a more uniform exit flow. However, a longer contraction costs more, and results in a thicker boundary layer. Figure 10 shows the velocity and pressure-gradient parameter near the contraction inlet, for a length of 24 inches, and a match point of 12 inches. The pressure-gradient parameter λ reaches a minimum of about -0.3, well beyond the nominal separation value of -0.09. These results are independent of Reynolds number, with the approximations used. Every 5th point is plotted, and the contraction begins at $x = 0$. The absolute values of the edge velocity are representative but not accurate; a linear scaling needs to be applied to show actual driver-tube freestream values.

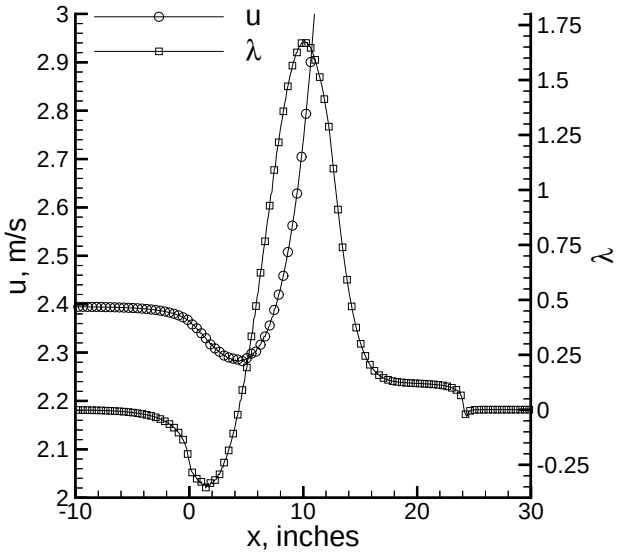

Figure 10: Boundary-Layer Properties near Inlet of 24-in. Contraction (mach6m1e)

Figure 11 shows similar results for a 36-inch contraction. The match point is again halfway, at 18 inches. The value of λ is less adverse, but still well beyond the marginal separation value of -0.09. Every 5th point is again shown. When the length is increased again to 48 inches, Figure 12 results. The match point is at 24-inches. Every point is now shown. The minimum value of λ is now about -0.05, indicating that the flow remains attached. The results of two different panelings are shown. The first, case 'v', has 1606 panels at an even 0.1-inch spacing. The second, case 'g', has 1636 panels at a spacing that varies by 40% with position. In both cases there is significant unevenness, especially in the derivatives, but the values of λ agree well enough to be useful. The unsmoothed edge velocities are always shown, unless otherwise indicated. Figure 13 shows unsmoothed and smoothed velocities, for the same

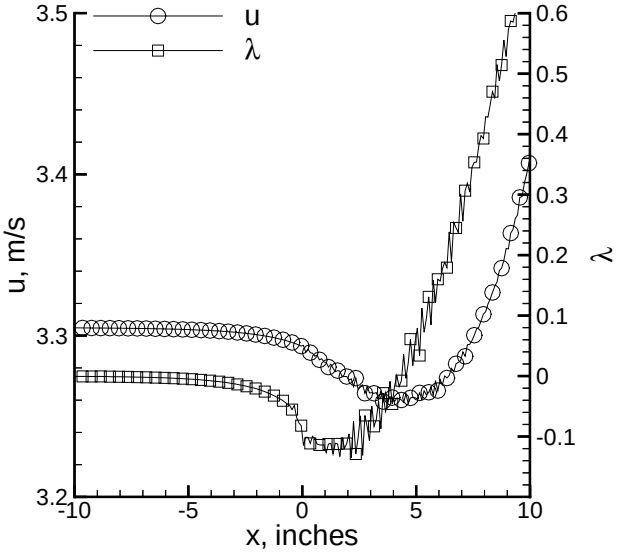

Figure 11: Boundary-Layer Properties near Inlet of 36-in. Contraction (mach6m1f)

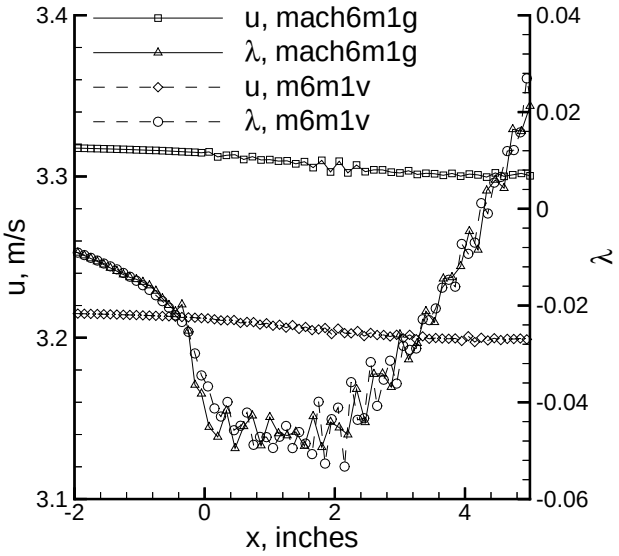

Figure 12: Boundary-Layer Properties near Inlet of 48-in. Contraction, Two Grids

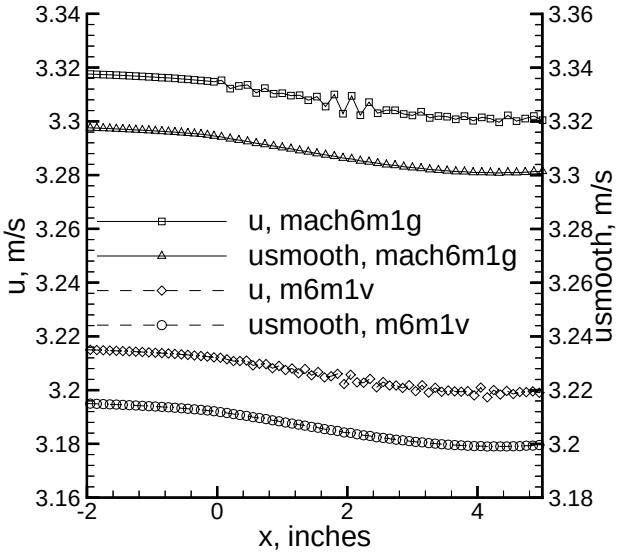

Figure 13: Effect of Smoothing on Velocities near Contraction Inlet

two cases, on offset scales, so that the effect of the smoothing can be seen.

Although the 48-inch contraction appears to avoid separation, it is rather long and expensive. A less expensive 40-inch contraction is shown in Figure 14. The minimum λ is now about -0.09, on the margin of separation. The match point is again halfway, at 20 inches.

Location of Match Point for Cubics

The effect of the match point location was then examined. Figure 15 shows results for another 40-inch contraction, with the match point moved downstream from 20 inches to 30 inches. The minimum λ has now improved to about -0.06. This contraction is longer than that suggested by the work of Morel, and the match point is best when farther downstream. Figure 16 shows the same contraction with two different panelings, again with good repeatability. Run `m6m1x2` has 1550 panels, spaced apart 0.035 inches in the slot area, 0.042 inches in the downstream end of the contraction, 0.125 inches in the upstream part of the contraction, and 0.1 inches in the inlet duct. Run `m6m1y2` has 1470 panels, spaced apart 0.035 inches in the slot, and 0.1 inches elsewhere. The irregularities in λ are again non-negligable but sufficiently small to allow reliable design.

Many of these contractions were analyzed in two ways. Figure 17 shows the 48-inch contraction, with a 24-inch match point. The lower pair of curves

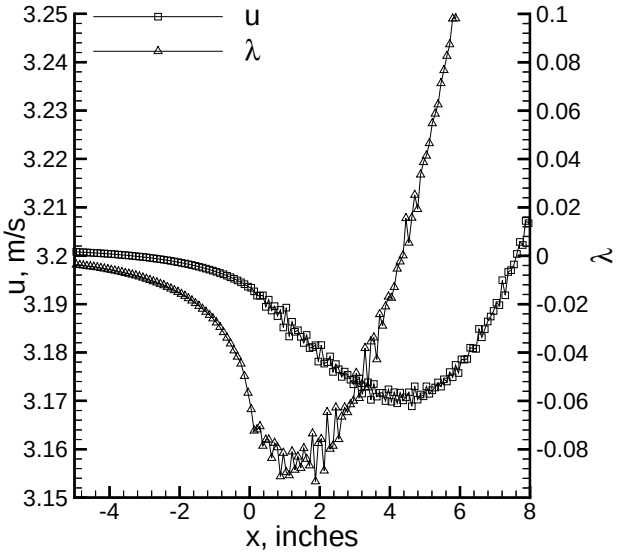

Figure 14: Boundary-Layer Properties near Inlet of 40-in. Contraction with 20-in. Match Point (m6m1w)

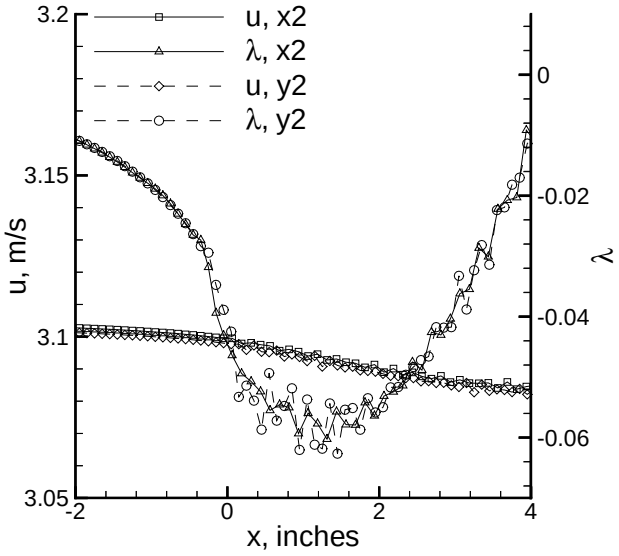

Figure 16: Boundary Layer Properties near Inlet of the Same 40-in. Contraction, with Two Panelings (m6m1x2,m6m1y2)

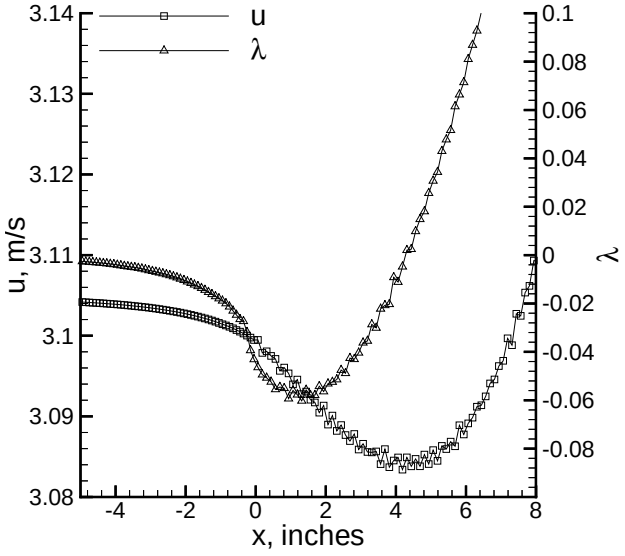

Figure 15: Boundary-Layer Properties near Inlet of 40-in. Contraction with 30-in. Match Point (m6m1x2)

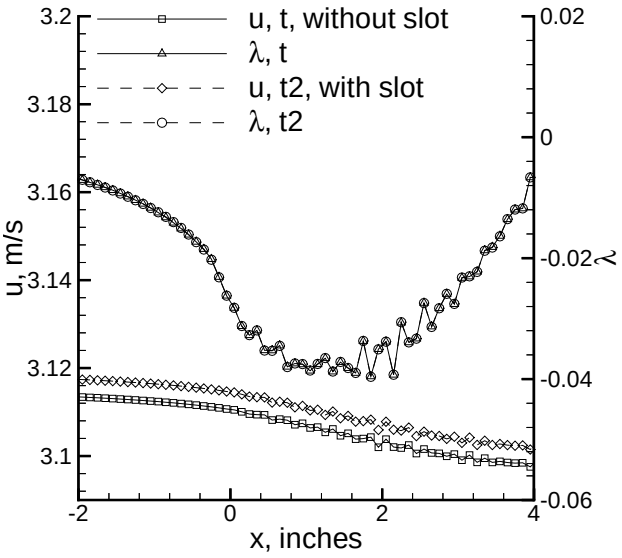

Figure 17: Boundary Layer Properties near Inlet of the Same 40-in. Contraction, Modeled in Two Ways

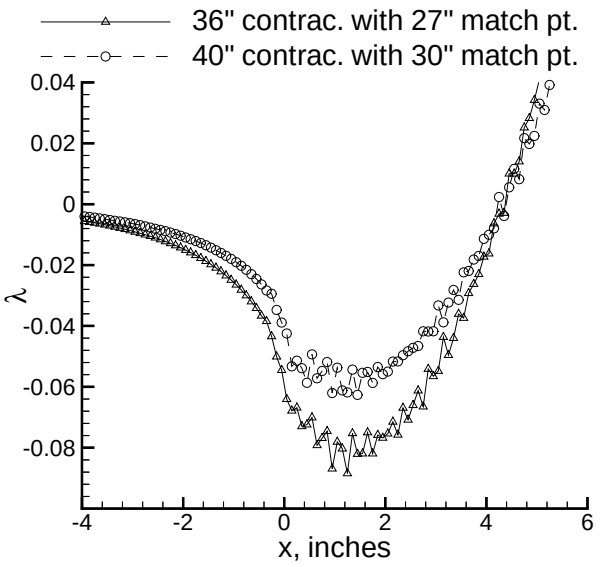

Figure 18: Boundary-Layer Properties near Inlet of Two Contractions with 75% Match Points (m6m1z2,m6m1y2)

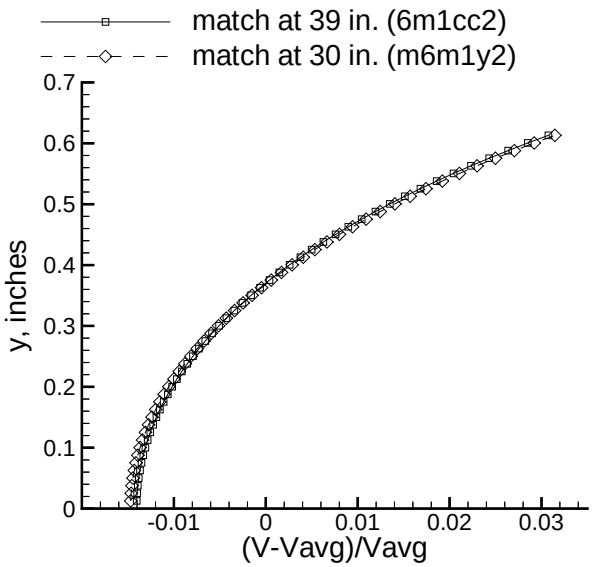

Figure 19: Profile of Mean Velocity Variations in Two 40-in. Contractions

models the full geometry with slot. The upper does not contain the slot, but gives a smooth contour past the slot location into the nozzle inlet. Since the slot is far downstream of the contraction inlet, an effect on the separation point there is not expected, and the figure shows in fact that the results for λ in the contraction inlet are almost identical. Runs `m6m1t and m6m1t2` differ from `mach6m1g` and `m6m1v` by having a third paneling: 1615 panels in the contraction wall, 0.035-in. spacing in the slot area, 0.05-in. in the downstream part of the contraction, 0.1-in. elsewhere; 394 panels in the lip, 0.035-in. spacing.

The downstream match point was then tried in a slightly shorter contraction, of 36-inches, with a match point again at 75%. Figure 18 shows the results. Even with the match point moved downstream, the 36-inch contraction is still marginal for separation. It appears that a 40-inch contraction will be necessary, with the match point somewhere around 75% of the distance to the exit.

The last series of computations tested the effect of moving the match point even further downstream. This continued to reduce the value of λ at the contraction entry, suggesting shorter contractions could be used. However, the geometry started to become rather unusual, and unforeseen problems were feared. The expected difficulty with a downstream match point is an increase in curvature near the downstream end, causing an increase in flow nonuniformity near the contraction exit, and an increase in the chance of boundary-layer separation there [23]. The usual difficulties will be modified for the present case, since boundary-layer suction is being used near the exit. Figure 19 shows the variation of the total velocity from the average for a profile just short of the nozzle throat, for two match points in 40-inch contractions. A 4% variation in the mean velocity can be seen, with the velocity slightly higher near the wall. Although this might seem rather high, a computation of the shorter Langley Mach-6 contraction yielded a 12% variation, and this nozzle has good mean flow [12]. However, further movement of the match point downstream could only shorten the contraction by another 10% or so, a marginal cost savings. Since the 40-inch contraction with the 30-inch match point could not be shortened much further without significant increases in perceived risk, it was selected for the final design.

Control of Separation at the Suction Bleed Lip

Figure 20 shows the surface velocity in the region near the bleed lip. To analyze an interior flow with the EOD code, the panels must be entered so that the flow is to the left, walking between successive panels [17, pp. 20-21]. The sign of the velocity is relative to the direction in which the panels are entered. The flow accelerates approaching the lip, which is located 0.015 inches upstream of $x = 40.0$. The lip is paneled in a clockwise fashion. The stagnation point is nearly at the forward tip of the nose.

Since the flow becomes transonic somewhat downstream of the bleed lip, the only important part

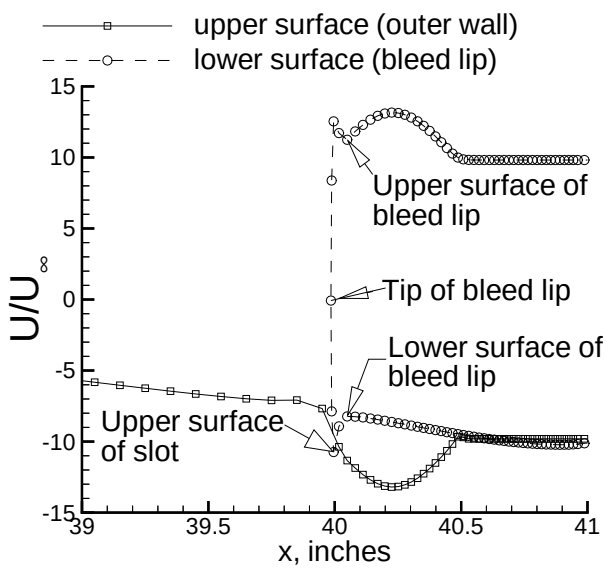

Figure 20: Surface Velocity near Bleed Lip (m6m1y2)

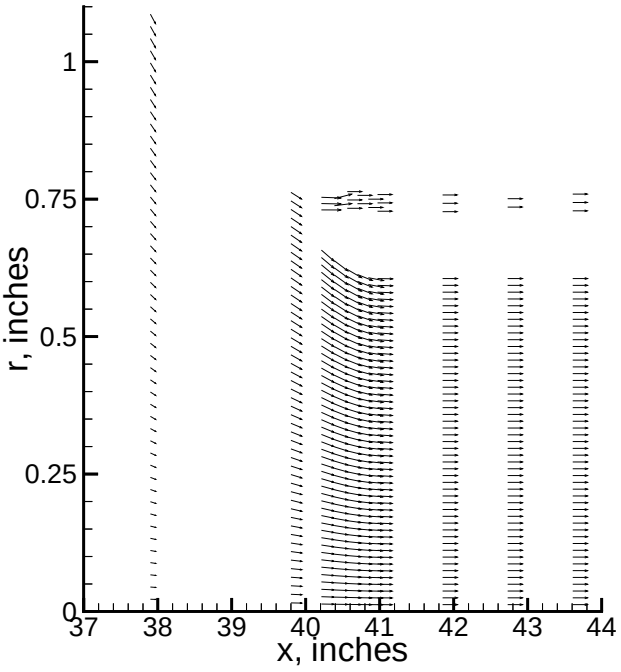

Figure 21: Flowfield Vector Velocities for Final Contraction (m6m1y2)

of the downstream computation is to set the correct massflow. The bleed slot contour downstream of the bleed-slot throat is therefore adjusted to a value which gives the correct massflow ratio in the slot. This requires the elimination of most of the expansion downstream of the slot minimum. For Figure 20, the slot width at the downstream end of the panels was chosen to give a slot massflow of 12.8% of the upstream massflow. This is slightly larger than the 10% planned during the design, which used the method of streamtubes. The total massflow in the computations is consistent to within 0.5%. In Figure 20 there is a very small region of sharp adverse gradient in the flow going around both sides of the hemispherical tip. This is to be expected, since it is well known that an unbounded flow separates when passing around a semi-circular nose attached to a 2D flat plate [17, Fig. 58]. *Thus, although not shown in their limited-accuracy computations, the flow* **must** *separate in passing over the 0.030-inch diameter semi-circular tips of the Langley Mach-6 and Mach-8 quiet nozzles.* However, since this tip is so small, the separated region is presumably very small, probably less than 0.1 inches long, and perhaps it has little effect. To eliminate the separation around a flat plate with an elliptical leading edge, it is necessary to go to an ellipticity of about 6 [17, 35]. It is not clear that this difficult machining job can be successfully performed, nor is it clear that it will make a significant difference.

In Figure 20, three curves are shown downstream of the bleed lip, at 40 inches. The top curve is the upper surface of the bleed lip (bottom of slot), and it matches the bottom curve, which is the upper surface of the slot. The signs are different because of the left-hand rule used in EOD to determine signs; the magnitudes agree well. The flow accelerates to the minimum and then decelerates. In the actual nozzle it is important that the flow be sonic at the slot minimum, so that the separations that will occur downstream cannot affect the upstream flow. This sonic throat will also set the actual massflow that passes through the slot. The flow on the lower surface of the bleed lip continues to accelerate smoothly into the main nozzle throat. The local adverse gradient around the lip is present only over about 0.050 inches.

Figure 21 shows velocity vectors plotted using the data printed at the massflow rake positions. The overall flow looks smooth.

The bleed slot flow quantity has the dominant effect on the position of the stagnation point on the bleed lip. Figure 22 shows the bleed slot flow for a 48-inch contraction with a 24-inch match point, in a case where the actual slot massflow was 9.25%, below the design value of 10%. Since the velocity at the lip tip is now negative, the stagnation point has moved above the center of the lip tip. The adverse gradient going around toward the main flow

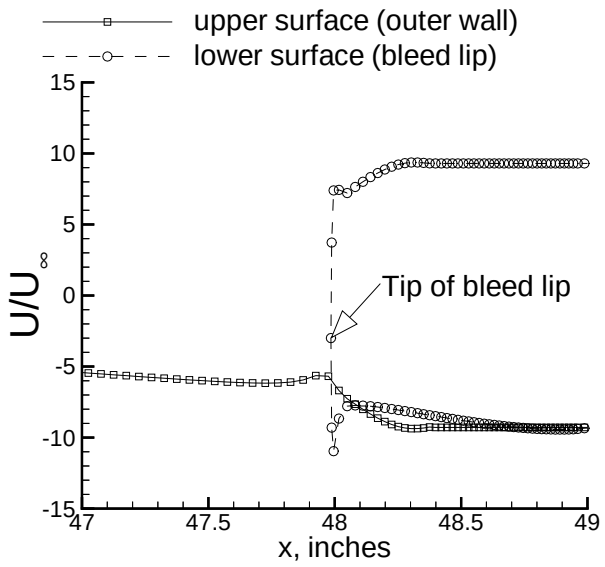

Figure 22: Bleed Lip Velocities for 48-in. Contraction with Reduced Slot Flow (m6m1m2)

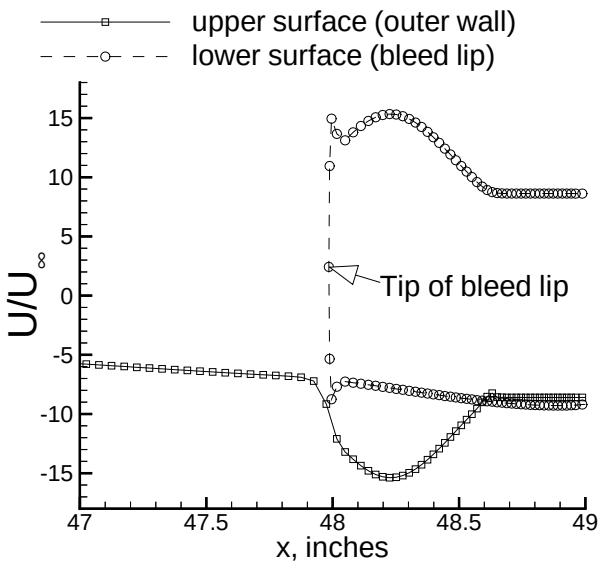

Figure 23: Bleed Lip Velocities for 48-in. Contraction with Increased Slot Flow (m6m1n2)

is slightly worse, in the limited resolution available. A decrease in slot massflow moves the separating streamline up, thereby moving up the stagnation point.

Figure 23 shows the same contraction, where the EOD exit geometry is adjusted to give a slot massflow of 15.8%. Here, the stagnation point is below the lip tip, since the velocity at the tip is positive. The adverse pressure gradient at the lower surface of the tip is slightly improved.

The only factor which seems to have a significant affect on the position of the bleed-lip stagnation point is the massflow through the slot. An attempt was made to move the stagnation point by changing the angle of the contraction as it approaches the tip, with almost no effect.

Mechanical Design of the Contraction

The mechanical design of the contraction and nozzle is shown in Figure 24.

The contraction is composed of 3 sections. The first two are 304 stainless steel, to match the low-cost material and the thermal expansion coefficient of the driver tube. The joint between the driver tube and the first contraction section is an o-ring flanged joint with two dowels. The end of the driver tube is slightly egg-shaped, with diameters that vary from 17.467 to 17.511. The contraction and driver-tube will be hand-finished to make a smooth joint. Downstream of this first joint, all joints are lapped. The nozzle is to be built from 15-5PH stainless steel, vacuum-arc remelted and heat-treated to condition H1100.

Figure 25 shows an assembly drawing of the throat region.

The last circular-arc section of the contraction is machined as a separate ring, allowing ready modification of the slot throat. This should allow changing the position of the stagnation point on the bleed lip. A dynamic pressure transducer will be mounted in the ring near the slot throat, to monitor the mean flow and fluctuations there. A commercial band heater is shown mounted on the back surface of the nozzle bleed lip. This enables raising the lip temperature above ambient, as required by the analysis in Ref. [36], without raising the temperature of the rest of the apparatus any more than needed.

Detailed Design of the Nozzle and Joints

Joint Design

To make the nozzle by boring solid blocks on a CNC lathe, the nozzle must be made in sections that are limited by the boring bar length. For a given machine, the longer the section, the fewer the joints, but the less accurately they can be made. The present design has a relatively large number of sections which can therefore be held to closer tolerances. In the present design, the first joint is located

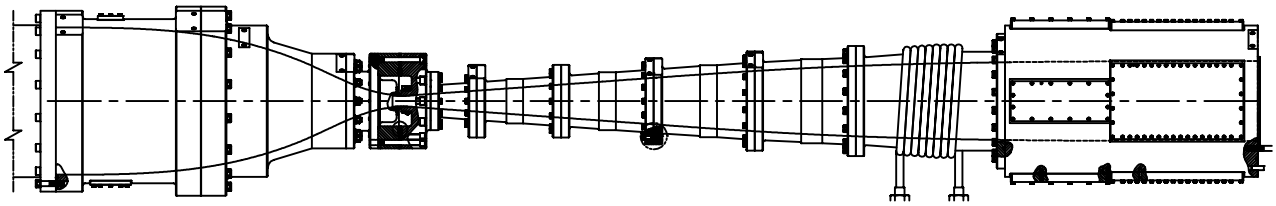

Figure 24: Assembly Drawing of Contraction and Nozzle

about 4.75 inches downstream of the bleed lip tip. As shown in Ref. [36], the allowable step at a joint here is about 0.0003 inches, for a 1000R heated wall, at 150 psi. Careful design and fabrication will be necessary to achieve this tolerance at the joint, and to maintain it even after numerous heating/cooling cycles. Although the first joint in the NASA Langley Mach-8 quiet nozzle was initially almost perfect, a step is now visible with a flashlight, according to Steve Wilkinson, and initial indications of the nozzle performance are disappointing.

Since the alternative to joints is a long electroformed nozzle, which would be much more expensive and also difficult, the joint problem is being addressed in detail. The current plan for machining the upstream sections of the nozzle is as follows:

1. Number the sections starting from section 1 at the throat, increasing downstream.

2. Rough machine section 1. Stress relieve carefully. Machine the final contour over section 1, except for the last 1/4-inch or so. Polish the section.

3. Rough machine section 2. Stress relieve carefully. Assemble to section 1, using a lap joint. Since a 0.001-inch interference fit is used, section 1 is cooled with liquid nitrogen to allow assembly, after which the joint is never separated.

4. Machine the final contour in section 1 and 2, feathering into the final contour already machined upstream. This must be done without damaging the 1 microinch polish in the upstream part of section 1.

5. Polish section 2.

6. Thermal cycle the two sections in an oven, checking the joint to make sure it remains smooth.

7. Repeat the process for sections 3 and 4. Beyond this point, the finish tolerances have relaxed so that a high quality disassembleable lap joint should not trip the boundary layer, although it may create small Mach waves in the mean flow which will have to be tolerated.

To assess the possibility of fabricating such a near-perfect joint, and of keeping it smooth, a test joint has been fabricated. Figure 26 shows an assembly view.

A single complete cycle of the process is being tested with this joint, which is complete through final machining. Unfortunately, the coordinate measurements are not yet available. If problems develop that are difficult to overcome, the upstream subassembly of the nozzle will have to be electroformed as a single unit.

Test Region of Nozzle

The nozzle is designed to have 8 sections, as can be seen in Figure 24. Since boundary-layer transition on the nozzle walls limits the downstream extent of the useful region of uniform flow, the test models are placed in the downstream end of the nozzle, immediately following the onset of uniform flow. The last section of the nozzle is thus the test region, as shown in Figure 27.

Rays showing the onset of noise radiated from transition on the nozzle wall are shown in the upper half. A 5-deg. half-angle cone at zero angle of attack is shown where it would be placed for measurements (although actual tests are planned to use primarily 3D models). The cone diameter is nearly the largest allowable, according to Pope's chart for certain start of blunt models [28, Fig. 1:27]. This fairly slender cone fits entirely within the nozzle, so the section downstream of the nozzle will have no windows – it will contain only a double-wedge second-throat centerbody that supports the model sting.

Figure 27 also shows two rectangular regions with rounded corners, that mark the upstream and downstream window locations. The upstream window extends upstream of the onset of uniform flow, to allow generating controlled disturbances using the laser perturber. The larger window downstream is

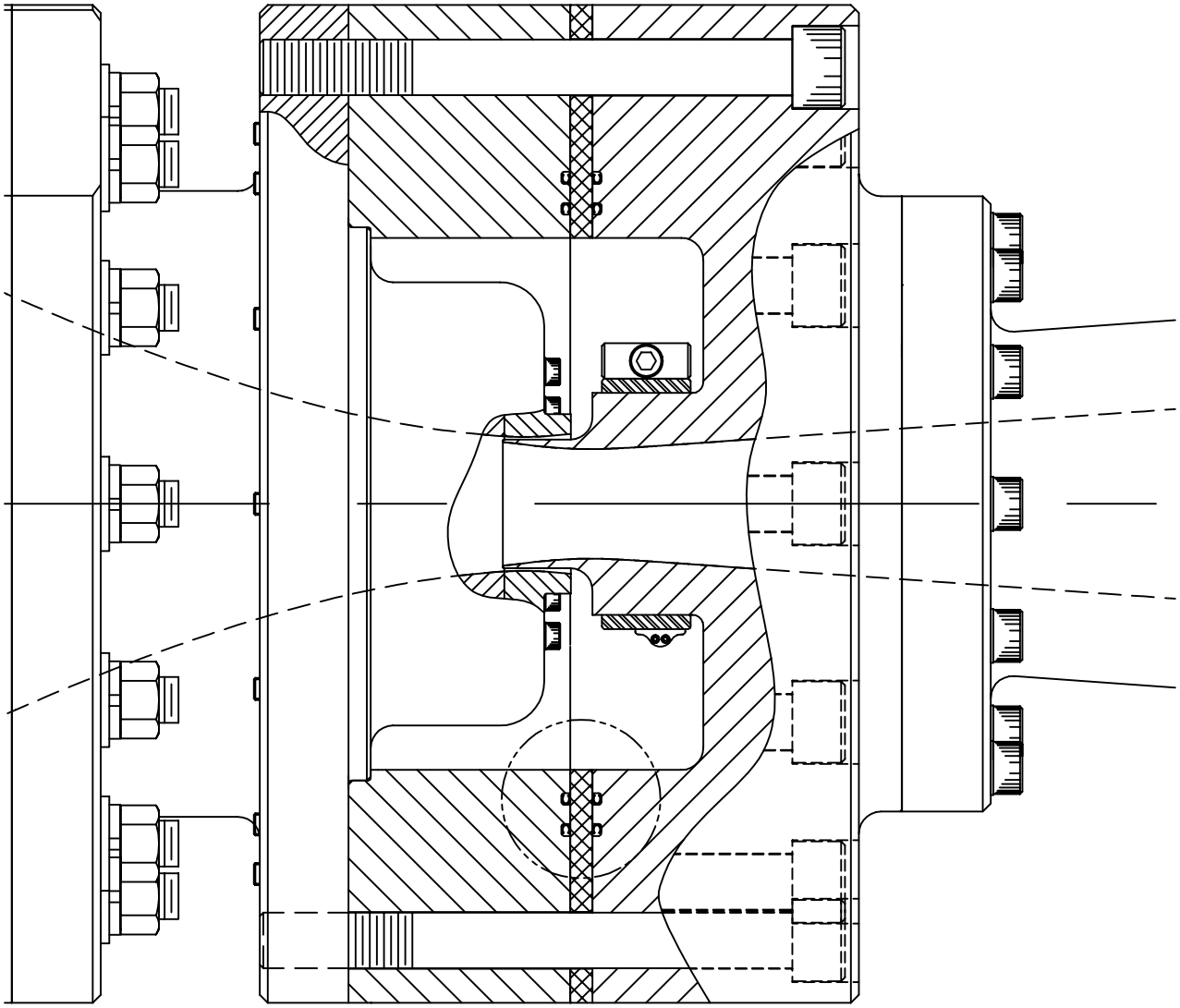

Figure 25: Assembly Drawing for the Nozzle Throat, Half Scale

the main window through which measurements will be made. Steel blanks will be installed initially, for shakedown; these can be modified to contain hot-wire traverses and other instrumentation. Figure 28 shows a cross-section of the nozzle in the middle of the downstream windows. The final wall thickness is about 4 inches, to provide great stiffness for the window mounting. The windows have an aspheric internal curvature, to match the nozzle i.d. They must also be thick, to hold the full stagnation pressure before the flow starts. Although the optical and manufacturing problems associate with this curvature seem readily solvable, no glass will be procured until the quiet-flow performance of the tunnel is determined using probes.

Summary

A Mach-6 quiet-flow Ludwieg tube has been designed and is being fabricated. The stainless-steel driver tube was fabricated to minimize steps and gaps, and the boundary layer is likely to remain laminar. The contraction has an area ratio of 133, to the bleed lip. It was designed using matched cubics, with an axisymmetric panel method code and the Rott-Crabtree laminar-boundary-layer analysis method. A length of approximately 2.3 inlet diameters is required to avoid laminar separation in the inlet. This length is substantially larger than that suggested by Morel [23], probably because he considered only turbulent separation, did not analyze the boundary layer explicitly, and considered much smaller area ratios.

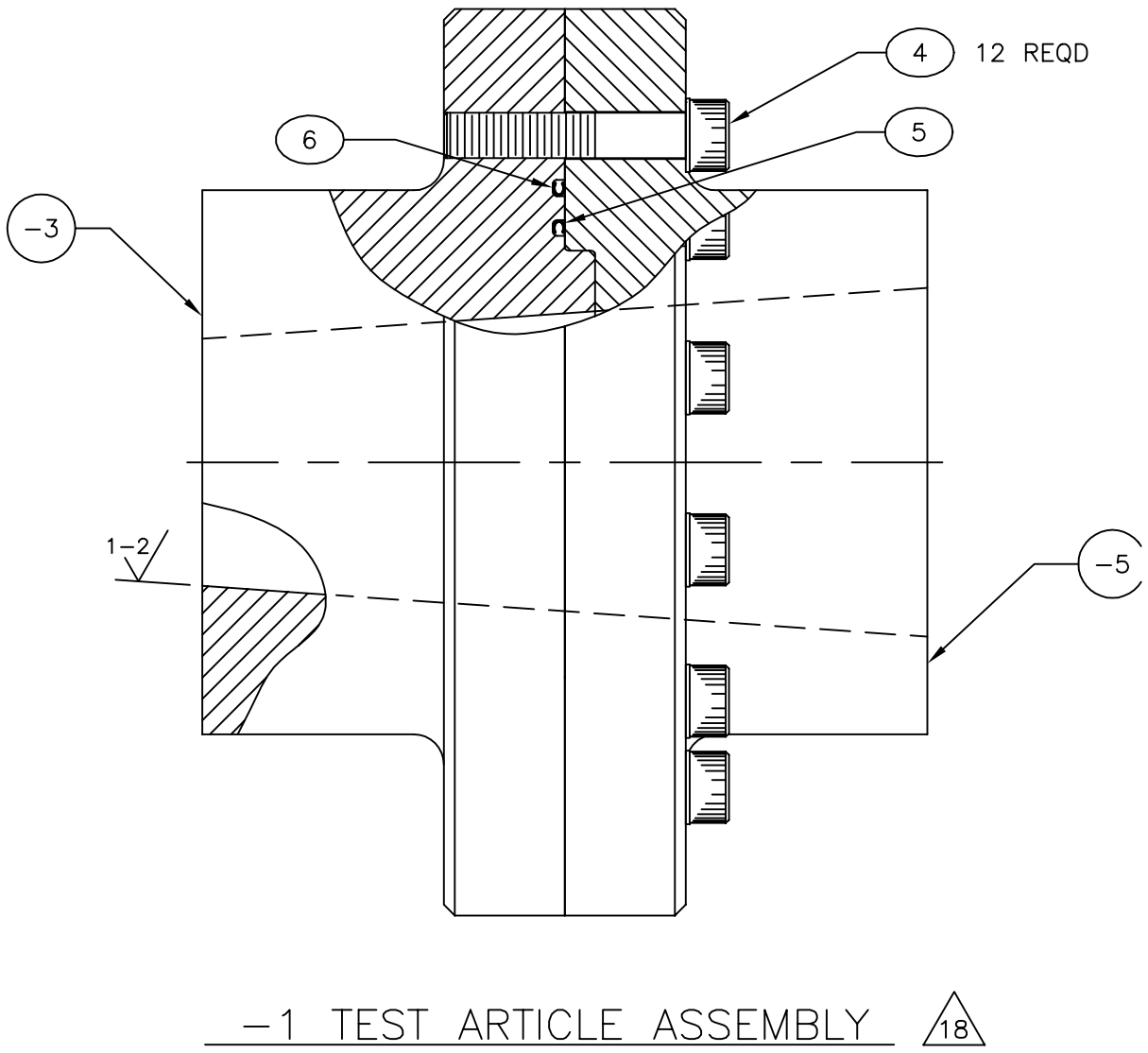

Figure 26: Test Joint Assembly, 2/3 Scale

The nozzle is to be machined in sections, requiring some nearly perfect joints near the throat. A test joint has been fabricated and awaits testing. The mechanical design is essentially complete, and the commencement of fabrication awaits successful completion of the test joint.

Acknowledgements

The work is funded by AFOSR under grants F49620-97-1-0037 and F49620-98-1-0284. The generous cooperation of the NASA Langley quiet tunnel group is appreciated. Matching funding for tunnel construction is being provided by a gift from the Boeing Company. The detailed mechanical design of the nozzle and contraction was carried out by Dynamic Engineering Inc., Newport News VA, under the supervision of Mr. Doug Weber. The EOD code was provided by Danny Hwang from NASA Lewis Research Center.

References

[1] AGARD, editor. *Sustained Hypersonic Flight*. AGARD, April 1997. CP-600, vol. 3.

[2] Timothy Alcenius, S.P. Schneider, Ivan E. Beckwith, and John J. Korte. Development of square nozzles for high-speed low-disturbance wind tunnels. Paper 94-2578, AIAA, June 1994.

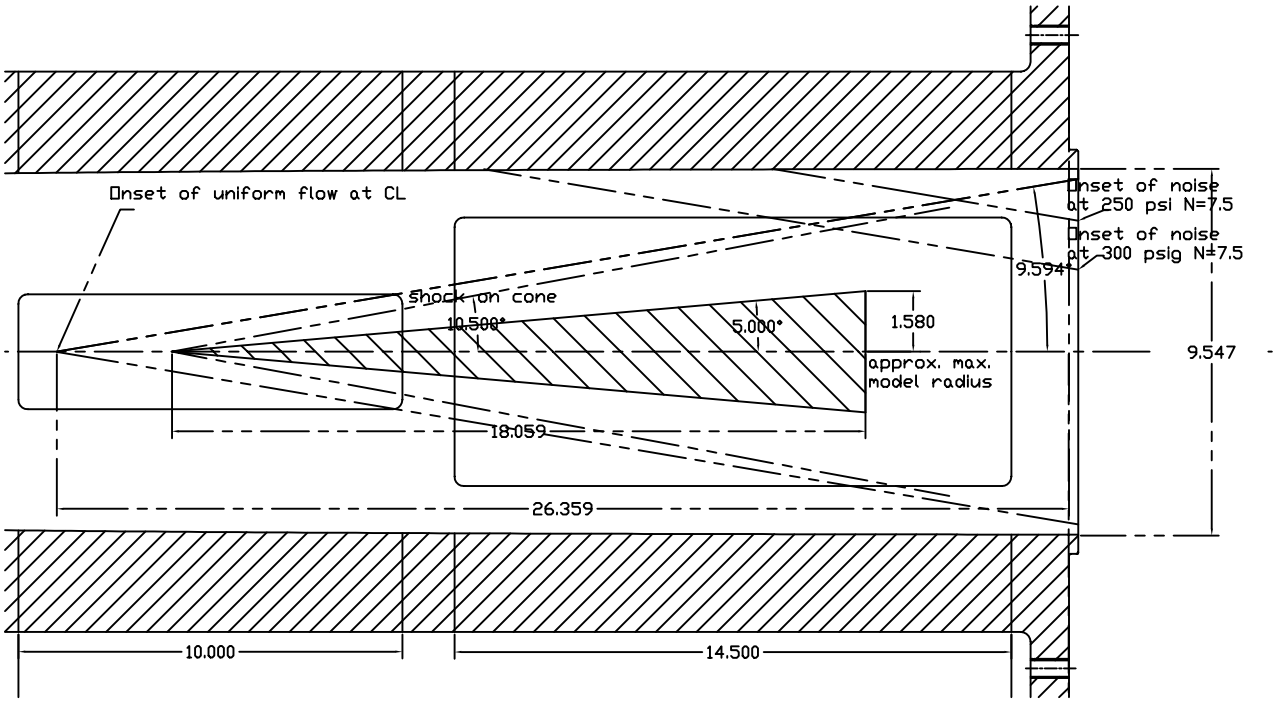

Figure 27: Last Nozzle Section, Sketched at 1/5 scale

[3] Yehia M. Amr and J. Gordon Hall. Stability limits and transition times of wave-induced wall boundary layers. In *13th International Symposium on Shock Tubes and Waves*, pages 280–288, Albany, New York, 1981. SUNY Press. NASA RECON citation 83A26151.

[4] J.B. Anders, P.C. Stainback, L.R. Keefe, and I.E. Beckwith. Fluctuating disturbances in a Mach-5 wind tunnel. Paper, AIAA, 1976. In the Proceedings of the 9th Aerodynamic Testing Conference, pp. 185-197.

[5] R. Balasubramanian. Converging slotted nozzle flow study. A manual for a modified version of the Strikwerda slotted nozzle code. Produced under contract NAS-1-19000, work order Q-005, Feb. 1990. Obtained from Steve Wilkinson at NASA Langley.

[6] J.-P. Barrand, J.-M. Dorvaux, and E. Rieutord. Pressure records analysis in an unsteady expansion wave. Paper 84-0633, AIAA, March 1984.

[7] E. Becker. Boundary layer in and behind an expansion wave. *Engineer Archives*, 25(3), 1957. Translated from German to English by David A. Russell, University of Washington.

[8] E. Becker. Unsteady boundary layers behind compression shocks and expansion waves. *Progress in Aeronautical Sciences*, 1:104–173, 1961. Translated from German to English by Associated Technical Services, Glen Ridge, NJ, 1969.

[9] I. Beckwith, F. Chen, S. Wilkinson, M. Malik, and D. Tuttle. Design and operational features of low-disturbance wind tunnels at NASA Langley for Mach numbers from 3.5 to 18. Paper 90-1391, AIAA, June 1990.

[10] I.E. Beckwith and C.G. Miller III. Aerothermodynamics and transition in high-speed wind tunnels at NASA Langley. *Annual Review of Fluid Mechanics*, 22:419–439, 1990.

[11] J.H. Bell and R.D. Mehta. Contraction design for small low-speed wind tunnels. Contractor Report CR-177488, NASA, August 1988.

[12] Alan E. Blanchard, Jason T. Lachowicz, and Stephen P. Wilkinson. NASA Langley Mach 6 quiet wind-tunnel performance. *AIAA Journal*, 35(1):23–28, January 1997.

[13] D. G. Friedman. Improved solution for potential flow about arbitrary axisymmetric bodies by the use of a higher-order surface source method. Part II. Users manual for computer program. Technical Report NASA-CR-134695, NASA, 1974.

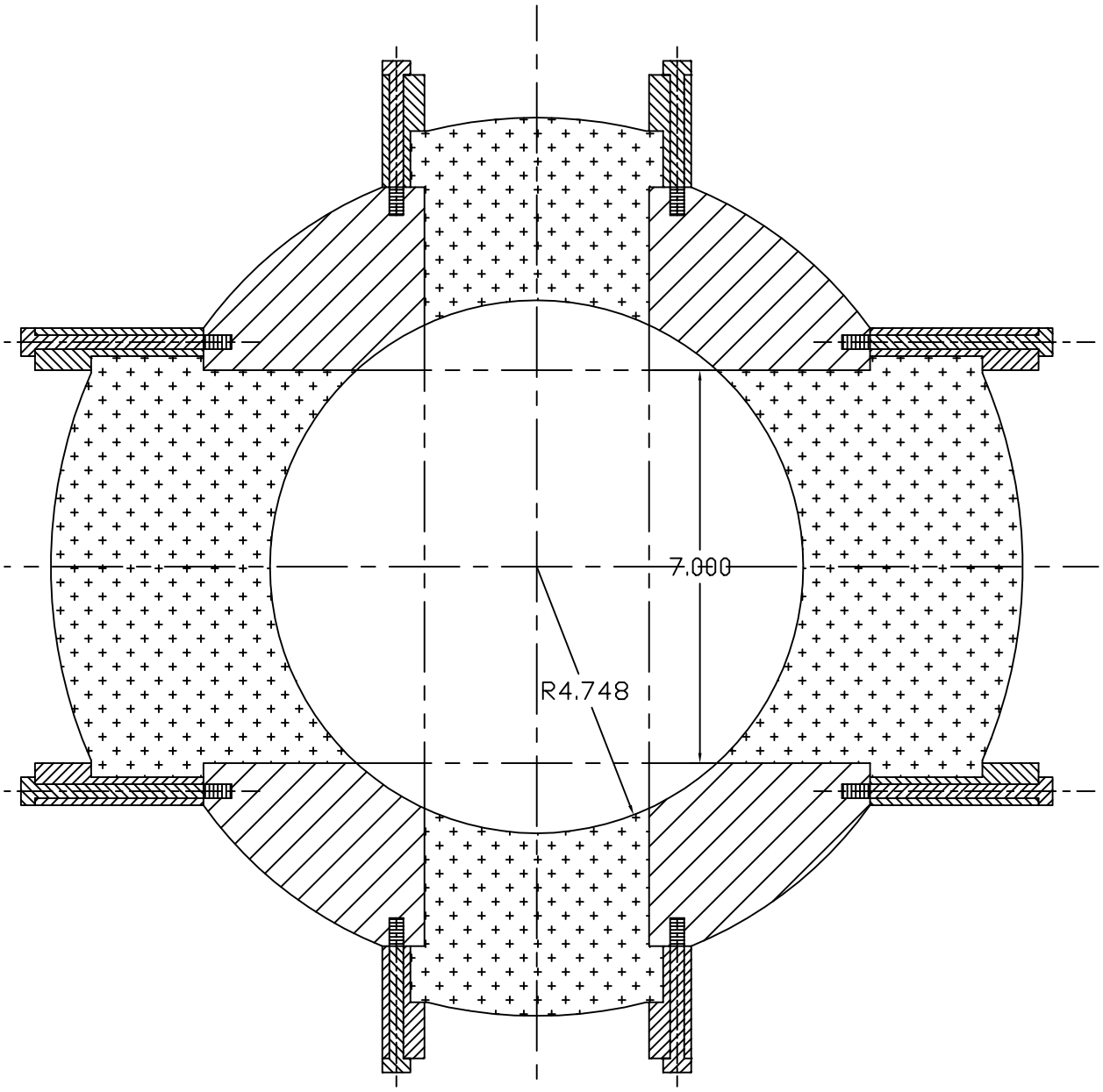

Figure 28: Sketch of Nozzle Cross-Section with Glass, at 1/3 Scale

[14] J. G. Hall. Laminar boundary layers developed within unsteady expansion and compression waves. *AIAA Journal*, 10(4):499–505, 1972.

[15] J.E. Harris and D.K. Blanchard. Computer program for solving laminar, transitional, or turbulent compressible boundary-layer equations for two-dimensional and axisymmetric flow. Technical Report NASA-TM-83207, NASA, February 1982.

[16] J. L. Hess and Jr. R. P. Martin. Improved solution for potential flow about arbitrary axisymmetric bodies by the use of a higher-order surface source method. Part I. Theory and results. Technical Report NASA-CR-134694, NASA, 1974.

[17] J. L. Hess and A.M.O. Smith. Calculation of potential flow about arbitrary bodies. *Progress in Aeronautical Sciences*, 8:1–138, 1967.

[18] Uwe G. Hingst. Laminar/turbulent flow transition effects on high speed missile domes. In *CP-493, Missile Aerodynamics*, pages 27–1 to 27–8. AGARD, 1990.

[19] H.A. Korejwo and M.S. Holden. Ground test facilities for aerothermal and aero-optical evaluation of hypersonic interceptors. Paper 92-1074, AIAA, February 1992.

[20] Dale W. Ladoon, John D. Schmisseur, and Steven P. Schneider. Laser-induced resonance in a forward-facing cavity at Mach 4. Paper 97-0339, AIAA, January 1997.

[21] Dale W. Ladoon and Steven P. Schneider. Measurements of controlled wave packets at Mach 4 on a cone at angle of attack. Paper 98-0436, AIAA, January 1998.

[22] J. Lukasiewicz. *Experimental Methods of Hypersonics*. Marcel-Dekker, 1973.

[23] Thomas Morel. Comprehensive design of axisymmetric wind tunnel contractions. Paper 75-FE-17, ASME, 1975.

[24] R. Narasimha and K.R. Sreenivasan. Relaminarization of fluid flows. *Advances in Applied Mechanics*, 19:221–309, 1979.

[25] E. Piltz. *Boundary-Layer Effects on Pressure Variations in Ludwieg Tubes*. PhD thesis, Darmstadt, Technische Hochschule, Fakultaet fuer Maschinenbau, 1971. NASA 71A34792. English translation available as NASA 74X77072, DTIC AD918580L.

[26] E. Piltz. Boundary-layer effects on pressure variations in Ludwieg tubes. *AIAA Journal*, 10:1095–1097, 1972.

[27] E. Piltz. Boundary-layer effects on pressure variations in Ludwieg tubes. Lecture Series 42, Von Karman Institute for Fluid Dynamics, January 1972. A 10-page article from the Lecture Series. NASA RECON 79N20995.

[28] A. Pope and K. Goin. *High-Speed Wind Tunnel Testing*. Wiley, New York, 1965.

[29] H. Reed, R. Kimmel, D. Arnal, and S. Schneider. Drag prediction and transition in hypersonic flow. In *Sustained Hypersonic Flight*. AGARD, April 1997. Paper C15 in CP-600, vol. 3. Also appears as AIAA Paper 97-1818, June 1997.

[30] D.A. Russell, G.S. Knoke, and J.C. Wai. Uniformity of Ludwieg tube flows. In *Modern Developments in Shock Tube Research, Proceedings of the 10th International Shock Tube Symposium, Kyoto*, pages 244–251, 1975.

[31] Terry R. Salyer, Laura A. Randall, Steven H. Collicott, and Steven P. Schneider. Use of laser-differential interferometer to study receptivity on a hemispherical nose at Mach 4. Paper 98-0238, AIAA, January 1998.

[32] J. Schmisseur, S.P. Schneider, and S.H. Collicott. Receptivity of the Mach-4 boundary layer on an elliptic cone to laser-generated localized freestream perturbations. Paper 98-0532, AIAA, January 1998.

[33] S. P. Schneider and C. E. Haven. Quiet-flow Ludwieg tube for high-speed transition research. *AIAA Journal*, 33(4):688–693, April 1995.

[34] S.P. Schneider. A quiet-flow Ludwieg tube for experimental study of high speed boundary layer transition. Paper 92-3885, AIAA, July 1992. Gives detailed design information for facility as constructed.

[35] Steven P. Schneider. *Effects of Controlled Three-Dimensional Perturbations on Boundary Layer Transition*. PhD thesis, Graduate Aeronautical Laboratories, California Institute of Technology, Pasadena, California, 1989.

[36] Steven P. Schneider. Design of a Mach-6 quiet-flow wind-tunnel nozzle using the e**N method for transition estimation. Paper 98-0547, AIAA, January 1998.

[37] Steven P. Schneider, Steven H. Collicott, J.D. Schmisseur, Dale Ladoon, Laura A. Randall, Scott E. Munro, and T.R. Salyer. Laminar-turbulent transition research in the Purdue Mach-4 quiet-flow Ludwieg tube. Paper 96-2191, AIAA, June 1996.

[38] Steven P. Schneider and Scott E. Munro. Effect of heating on quiet flow in a Mach 4 Ludwieg tube. *AIAA Journal*, 36(5):872–873, May 1998.

[39] R.F. Starr and C.J. Schueler. Experimental studies of a Ludwieg tube high Reynolds number transonic tunnel. Paper 73-212, AIAA, January 1973.

[40] John Strikwerda. A time-split difference scheme for the compressible Navier-Stokes equations with applications to flows in slotted nozzles. CR 195970, NASA, 1980. 94N71978.

[41] Kwok-On Tong and David A. Russell. Viscous effects in tube flow initiated by an expansion wave. *AIAA Journal*, 15(12):1763–1769, December 1977.

[42] Frank M. White. *Viscous Fluid Flow*. McGraw-Hill, second edition, 1991.

[43] S. P. Wilkinson, S. G. Anders, and F.-J. Chen. Status of Langley quiet flow facility developments. Paper 94-2498, AIAA, June 1994.

[44] S.P. Wilkinson, S.G. Anders, F.-J. Chen, and I.E. Beckwith. Supersonic and hypersonic quiet tunnel technology at NASA Langley. Paper 92-3908, AIAA, July 1992.

[45] Stephen P. Wilkinson. A review of hypersonic boundary layer stability experiments in a quiet Mach 6 wind tunnel. Paper 97-1819, AIAA, June 1997.